Enhanced Methane Emissions during Amazonian Drought by Biomass Burning

Makoto Saito*[☯], Heon-Sook Kim[☯], Akihiko Ito, Tatsuya Yokota, Shamil Maksyutov

Center for Global Environmental Research, National Institute for Environmental Studies, 16-2 Onogawa, Tsukuba, Ibaraki 305-8506, Japan

[☯] These authors contributed equally to this work.
* saito.makoto@nies.go.jp

Abstract

The Amazon is a significant source of atmospheric methane, but little is known about the source response to increasing drought severity and frequency. We investigated satellite observations of atmospheric column-averaged methane for the 2010 drought and subsequent 2011 wet year in the Amazon using an atmospheric inversion scheme. Our analysis indicates an increase in atmospheric methane over the southern Amazon region during the drought, representing an increase in annual emissions relative to the wet year. We attribute the increase to emissions from biomass burning driven by intense drought, combined with carbon monoxide showing seasonal variations corresponding to methane variations. We show that there is probably a strong correspondence between drought and methane emissions in the Amazon.

Introduction

The Amazon region plays an important role in the global carbon cycle as a large and dynamic reservoir of organic carbon stored in forest biomass and soil [1], and as a significant source of atmospheric methane (CH_4), accounting for $\sim 10\%$ of atmospheric contributions globally [2]. The Amazon region suffered severe droughts in 2005 and 2010, caused by factors related to higher than average sea surface temperatures in the tropical North Atlantic, weaker trade winds, lower than average water vapor transport into the southern Amazon region, and a weakening of upward atmospheric flow over the region [3]. The drought events illustrate the vulnerability of forests to climate variations and the impact of intense moisture deficits on canopy structure, leading to a significant net loss of carbon [4]. The risk and occurrence of high-intensity forest fires is increased during droughts, thus accelerating carbon emissions [5]. Carbon dioxide (CO_2) emitted to the atmosphere is balanced in part by subsequent regrowth of vegetation, whereas CH_4 release is not. Climate models predict that the intensity and frequency of Amazonian droughts will increase rapidly in the 21st century [6]. Therefore, analyses of the 2005 and 2010 droughts could provide a better understanding of the role of Amazonian forests in the global carbon cycle under near-future climate conditions.

Amazonian wetlands are a primary source of atmospheric CH_4 [7]. The Amazonian CH_4 budget includes multiple sources and sinks (i.e., rivers and upland soils) whose contributions

are sensitive to feedback from drought conditions. Field measurements under experimental drought conditions provide estimates of the degree of sensitivity on some sources. However, significant gaps remain in our understanding of how CH_4 budgets in the Amazon region will respond to drought events, in part because observations representative of the entire region are lacking, which are required to reliably assess regional-scale CH_4 budgets.

Here, we examine the relative importance of drought on the CH_4 budget in the Amazon region, with a focus on major emission sources. We used retrieved atmospheric column-averaged CH_4 (XCH_4; V02.21) levels from Greenhouse gases Observing SATellite (GOSAT) measurements [8] for 2010 and 2011; in 2010, the Amazon experienced a severe drought, whereas 2011 was relatively wet [5]. The GOSAT measurements provide uniform global coverage and thus show a standardized distribution of CH_4 concentrations over the Amazon (Fig 1a), allowing an assessment of potential impacts of Amazonian drought on the CH_4 budget.

Methods

Using a Bayesian inversion scheme, surface CH_4 flux estimates for 43 regions globally were optimized by matching XCH_4 retrievals and surface observations. We excluded the northern Amazon region from the analyses because only a few XCH_4 retrievals were obtained for this region, owing to the presence of stationary clouds (Fig 1a). However, the signature of the 2010 drought remained strong in the XCH_4 retrieval data, as the 2010 drought was particularly severe in the southern Amazon region (Fig 1b).

Overview of GOSAT measurements

The GOSAT has been monitoring atmospheric CO_2 and CH_4 concentrations from space since its launch in January 2009 [11]. Measurements are taken by an onboard Thermal And Near-infrared Sensor for carbon Observation (TANSO), consisting of a Fourier Transform Spectrometer (FTS) and a Cloud and Aerosol Imager (CAI) [12]. The TANSO-FTS observes intensities of sunlight reflected or emitted from the Earth's surface and atmosphere in four spectral bands: 0.758–0.775, 1.56–1.72, 1.92–2.08, and 5.5–14.3 μm. The nadir footprint diameter of the TANSO-FTS is 10.5 km. The TANSO-CAI records an image of the atmosphere and the Earth's surface in four spectral bands, from the near-ultraviolet to near-infrared: 0.370–0.390, 0.664–0.684, 0.860–0.880, and 1.56–1.65 μm, at spatial resolutions of 0.5, 0.5, 0.5, and 1.5 km, respectively. The TANSO-CAI data are used for cloud screening of the TANSO-FTS data. We used XCH_4 values from short-wavelength infrared radiance spectra from TANSO-FTS bands 1–3 [8].

Atmospheric inversions

Surface CH_4 flux estimates are optimized to detect atmospheric CH_4 concentrations by minimizing the difference between observed and modeled values, $J(\mathbf{s})$, using a Bayesian inversion:

$$J(\mathbf{s}) = \frac{1}{2}\{(\mathbf{z} - \mathbf{H}\mathbf{s})^{\mathrm{T}}\mathbf{R}^{-1}(\mathbf{z} - \mathbf{H}\mathbf{s}) + (\mathbf{s} - \mathbf{s_p})^{\mathrm{T}}\mathbf{Q}^{-1}(\mathbf{s} - \mathbf{s_p})\} \tag{1}$$

where $\mathbf{z}$ represents an observation vector; $\mathbf{H}$ is a matrix of response at each measurement site to emissions from each region; $\mathbf{s}$ and $\mathbf{s_p}$ are vectors of estimated and a priori estimated regional fluxes, respectively; $\mathbf{R}$ and $\mathbf{Q}$ are error covariance matrices for the model–data mismatch and a priori flux, respectively; and T is the transpose of a matrix. The elements of $\mathbf{H}$ were calculated using the atmospheric tracer transport model NIES-TM [13]. The vector of the posterior flux
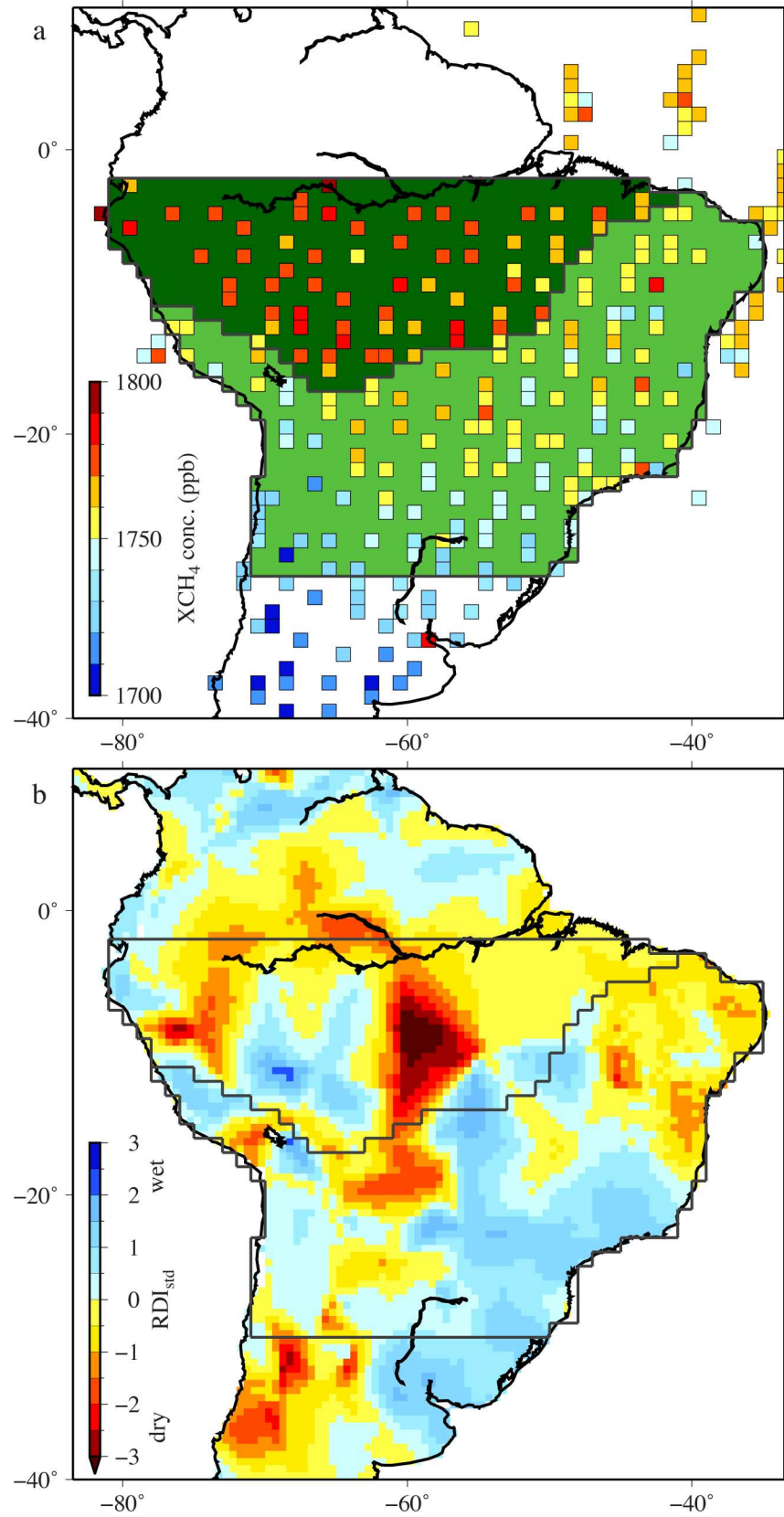
Fig 1. (a) Distribution of averaged concentrations of XCH$_4$ (ppb) from observational data acquired by GOSAT for August and September 2010 at a 1˚ × 1˚ grid resolution, with 479 and 1582 observed concentrations for the southern Amazon and central South America regions, respectively. The two regions analyzed are shown in dark green (southern Amazon region) and light green (central South America region). (b) Distribution of the standardized Reconnaissance Drought Index (RDI$_{std}$) in October 2009–September 2010 calculated using the method of [9] with monthly precipitation and potential evapotranspiration data from the Climate Research Unit (CRU), University of East Anglia, United Kingdom, using 0.5˚ × 0.5˚ mean monthly climatology CRU TS3.22 [10]. Both XCH$_4$ concentrations and RDI$_{std}$ values are color coded.

$\mathbf{s}'$ and its covariance matrix $\mathbf{Q}'$ are given by

$$\mathbf{s}' = \mathbf{s_p} + (\mathbf{H}^{\mathrm{T}}\mathbf{R}^{-1}\mathbf{H} + \mathbf{Q}^{-1})^{-1}\mathbf{H}^{\mathrm{T}}\mathbf{R}^{-1}(\mathbf{z} - \mathbf{Hs}) \tag{2}$$

$$\mathbf{Q}' = (\mathbf{H}^{\mathrm{T}}\mathbf{R}^{-1}\mathbf{H} + \mathbf{Q}^{-1})^{-1} \tag{3}$$

The inverse matrices in Eqs (2) and (3) were solved using LU factorization. We estimated monthly CH$_4$ fluxes for 43 regions, including 42 land regions at a sub-continental scale and one global ocean region (Fig A in S1 File). A detailed description of the inversion scheme is given by [14].

Observations of single-shot XCH$_4$ retrievals and individual ground-based observations from the World Data Center for Greenhouse Gases (WDCGG) [15] and a monitoring project of greenhouse gases over Siberia [16] were integrated in the inversion (Fig B in S1 File). Biases in XCH$_4$ retrievals were corrected to latitudinal and monthly ground-based observations using a second-order polynomial approximation [17] (the mean bias was assumed to be -5.9 ppb, with a standard deviation of 12.6 ppb (V02.XX) [8]). The uncertainty of the XCH$_4$ retrievals was set as the difference from the polynomial, with a minimum value of 12 ppb [18]. The uncertainties of the ground-based observation data were given by the mean residual standard deviation (RSD) of the GLOBALVIEW-CH$_4$ 2009 dataset [19], with minimum values of the flask sampling and continuous measurement data set as 6 and 20 ppb, respectively.

The inversion scheme consists of the NIES-TM, a module for CH$_4$ destruction processes caused by hydroxyl free radicals (OH) [20], and a fixed-lag Kalman smoother with a 4-month lag window [21]. The NIES-TM was implemented using a 2.5˚ × 2.5˚ horizontal grid resolution and 32 vertical levels, using a hybrid sigma-isentropic coordinate system. The NIES-TM was driven using 6-hourly climate forcings from the Japan Meteorological Agency Climate Data Assimilation System (JCDAS) [22].

The a priori fluxes were composed of three groups of emission sources: anthropogenic, natural, and biomass burning (Table A in S1 File). The anthropogenic sources were based on the emission inventories of the Emission Database for Global Atmospheric Research (EDGAR) v4.2 [23], and include fuel combustion and fugitive emissions from fuels, industrial processes, and product use, as well as agricultural sources, including animal waste and enteric fermentation, waste treatment, and fossil fuel fires, but excluding rice paddies. Natural sources include emissions from wetlands, rice paddies, and soil sources and sinks, which were based on the Vegetation Integrative SImulator for Trace gases (VISIT) terrestrial biosphere model [24], and also include emissions from termites, which were based on the tracer transport model GISS [25]. Biomass burning was based on the Global Fire Emissions Database (GFED) v3.1 product [26]. The a priori monthly fluxes of these three source groups were prepared at a 1˚ × 1˚ spatial resolution, and each group was optimized for the 43 regions in the inversion scheme. Uncertainties in the a priori fluxes were set to 20% of the values for the anthropogenic and biomass

burning sources and 50% for the natural sources. After inversion, the optimized emission sources in the four regions (Numbers 9, 10, 15 and 16 in Fig A in S1 File) of South America were aggregated over two large regions: the southern Amazon and central South America.

Results and Discussion

The dry season in the southern Amazon occurs between July and October. The largest positive temperature and the largest negative precipitation anomalies between 2010 and 2011 occurred in August and September 2010 [5]. The XCH_4 retrievals for this period show strong latitudinal gradients (Fig 1a) due to differences between CH_4 emission rates in the Northern and Southern Hemispheres. This agrees with previous measurements from the SCanning Imaging Absorption SpectroMeter for Atmospheric CHartographY (SCIAMACHY) satellite [27]. As confirmed by *in situ* surface measurements [28], longitudinal gradients were also observed in the XCH_4 retrievals. In the southern Amazon, low-level northeasterly air flows were dominated by year-round trade wind inflows across the northeastern coast of Brazil, flowing from the tropical North Atlantic region [29]. Levels of CH_4 in the southern Amazon were generally enhanced compared with those in the central South America region, indicating the contributions of upwind emission sources.

Fig 2 shows the relative effects of drought on atmospheric CH_4 concentrations, by comparing the variability of XCH_4 with that of a background region. The Atlantic area between 0–20˚S and 20–50˚W was determined as the background region for the dominant trade wind. After comparing XCH_4 with the background observations to obtain the relative effects (ΔXCH_4), we found a statistically significant difference ($P < 0.01$) between the XCH_4 variability for July–October in 2010 and 2011 in both the southern Amazon and the central South America regions. Monthly averaged ΔXCH_4 values increased from July to September 2010 in both regions, with median ΔXCH_4 values of +14.8 and +7.6 ppb for the southern Amazon and the central South America regions, respectively. In contrast, during 2011 the ΔXCH_4 levels increased in the southern Amazon region in August and decreased in September. Additionally, in the central South America region, changes in ΔXCH_4 levels during 2011 were not detectable. The analysis suggests that the 2010 drought enhanced CH_4 emissions in the southern Amazon region.

The inverse model shows that differences in XCH_4 variability between 2010 and 2011 were closely related to year-to-year changes in emissions from biomass burning (Fig 3). In the southern Amazon region, estimated CH_4 emissions from biomass burning during 2010 were six times higher than in 2011 (7.0 ± 1.0 versus 1.1 ± 0.2 Tg CH_4 yr^{-1}, respectively, or alternatively given as 1.46 ± 0.21 versus 0.24 ± 0.04 g CH_4 m^{-2} yr^{-1}, respectively). This resulted in a 22% increase in annual CH_4 fluxes in 2010 relative to those in 2011 (26.6 ± 7.5 versus 21.8 ± 6.4 Tg CH_4 yr^{-1}, respectively) despite a reduction in natural emissions (16.5 ± 6.0 versus 17.5 ± 5.6 Tg CH_4 yr^{-1}, respectively) and no changes in anthropogenic emissions (3.2 ± 0.5 Tg CH_4 yr^{-1}). Enhanced emissions from biomass burning were also detected in the central South America region in 2010 compared with 2011 (1.5 ± 0.3 verses 0.5 ± 0.1 Tg CH_4 yr^{-1}, respectively), but a comparable increase in annual CH_4 fluxes in 2010 (43.9 ± 11.2 Tg CH_4 in 2010 verses 45.0 ± 10.9 in 2011 Tg CH_4) was not discernable because 2011 included increased natural emissions. Annual CH_4 fluxes over the northern Amazon region in 2010 and 2011 were estimated as 23.9 and 23.0 Tg CH_4 yr^{-1}, respectively, for reference. In 2010, the posterior fluxes led to increases in total emissions of 17% and 9% in the southern Amazon and the central South America regions, respectively, compared with the a priori fluxes (22.6 ± 8.7 and 40.0 ± 13.6 Tg CH_4 yr^{-1}, respectively) (Table A in S1 File).
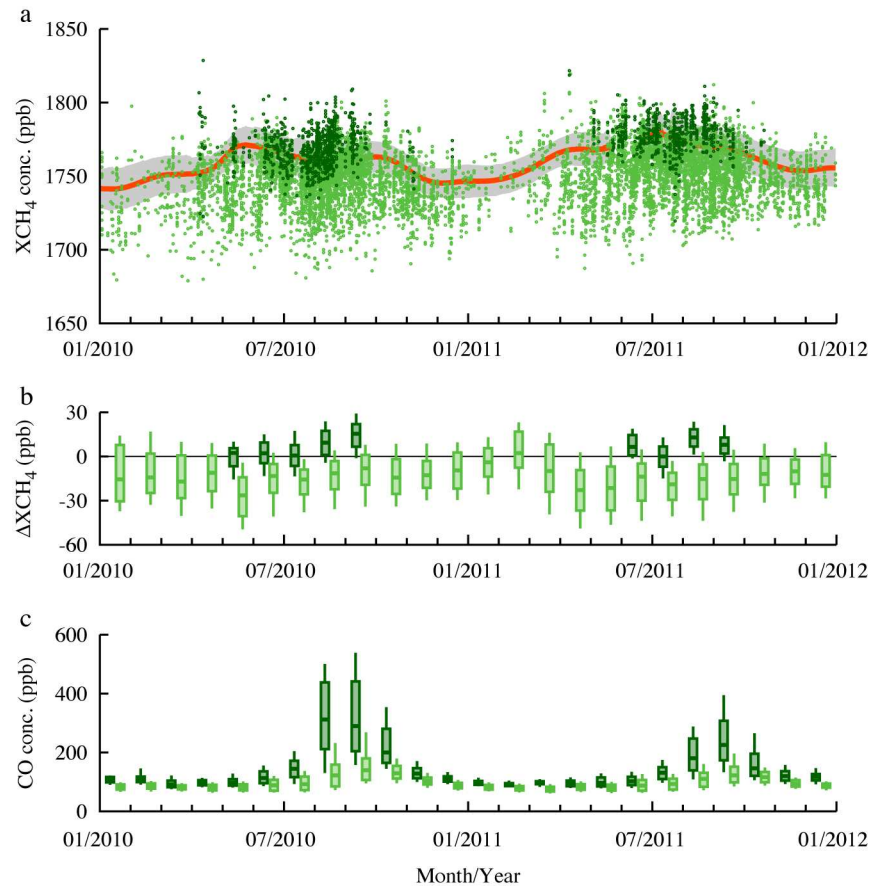
Fig 2. Time series of CH₄ and CO concentrations for 2010 and 2011. (a) Variability in XCH_4 concentrations (ppb) in the southern Amazon region (dark green circles), central South America region (light green circles), and background region (ocean area between 0˚–20˚S and 20˚–50˚W; red line). Daily data of the background region were constructed from discrete XCH_4 data using a Humming window with a window-width of 80 days. The standard errors (one sigma) of XCH_4 data are given by the gray boundary. The discontinuity at the background region for May 22–June 20 in 2011 reflects a lack of XCH_4 data. (b) Monthly variability in XCH_4 values (ppb) with the background subtracted (ΔXCH_4) in the southern Amazon region (dark green box-and-whiskers) and the central South America region (light green box-and-whiskers). Upper and lower values of the boxes are monthly quartiles of ΔXCH_4, bars through the boxes are medians, and whiskers represent the range of the 10th and 90th percentiles (data are not shown for months in which the number of data points was <25). (c) Same as (b), but showing surface CO concentrations (ppb) from the MOPITT L3 product.

doi:10.1371/journal.pone.0166039.g002

In the southern Amazon region, the CH₄ emission rate from biomass burning in 2010 exceeded previous estimates for the Legal Amazon region between 1992 and 1993 of 0.84 g $CH_4 \, m^{-2} \, yr^{-1}$ [30], and for the northern Amazon in 2001–2005 of 0.20 g $CH_4 \, m^{-2} \, yr^{-1}$ (assuming that fire occurs on one third of the days during the 4-month-long dry season) [28], and are comparable to local-scale emissions for primary Amazonian forest between 1986 and 1992 (~ 2 g $CH_4 \, m^{-2} \, yr^{-1}$) [31]. Recently [32] estimated the biomass burning emission in the southern Amazon region during 2010 to be 6.8 Tg $CH_4 \, yr^{-1}$, using a CH₄ assimilation system CarbonTracker-CH₄. Additionally, [33] reported the biomass burning emission of the Amazon Basin during 2010 and 2011 to be 5.4 and 0.5 Tg $CH_4 \, yr^{-1}$, respectively, based on the GFED v3.1 product.
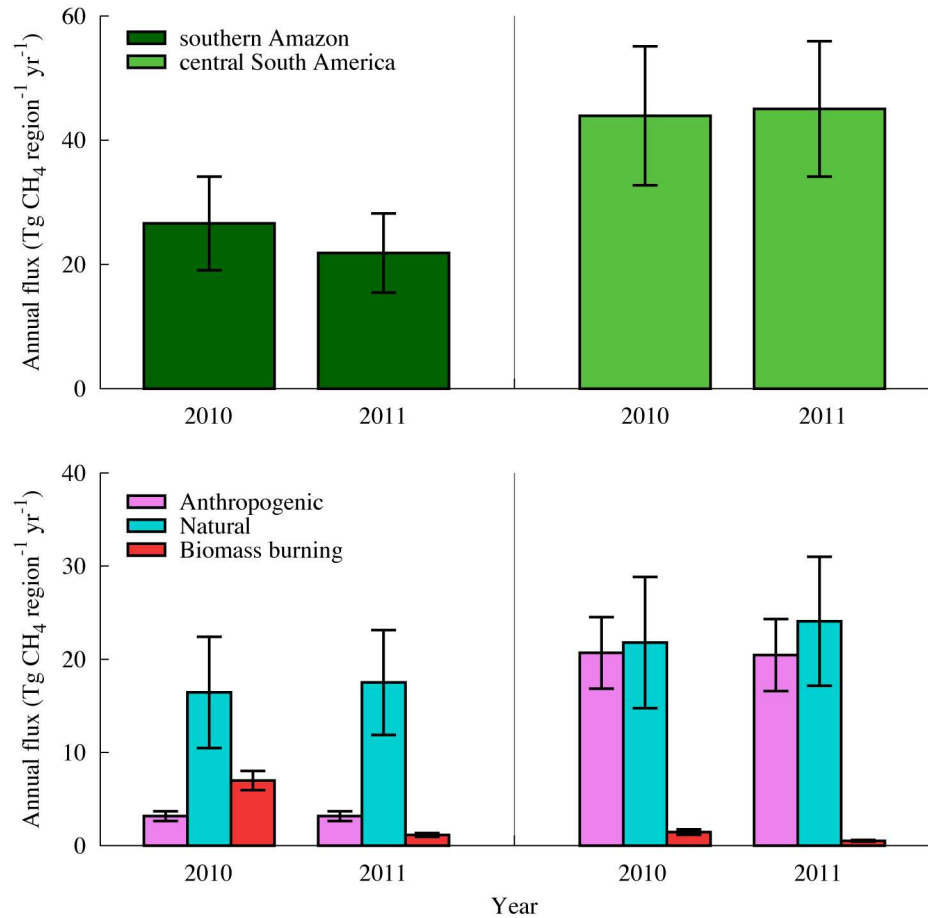
Fig 3. Total annual CH$_4$ flux (upper) and relative contributions of anthropogenic (magenta), natural (blue), and biomass-burning (red) fluxes (lower) in the southern Amazon region (left) and central South America region (right) for 2010 and 2011 (in Tg CH$_4$ region^{-1} yr^{-1}). Error bars represent flux uncertainties.

doi:10.1371/journal.pone.0166039.g003

The probability distribution for XCH$_4$ estimated with these posterior fluxes (PST) for 2010–2011 was compared with XCH$_4$ retrievals using the χ^2 goodness-of-fit test, as well as those estimated with a priori fluxes (APR) and posterior fluxes for inversion using ground-based observations only (GB) (Fig C in S1 File). The test for XCH$_4$ was divided into 14 classes and yields χ^2 = 151,643 for XCH$_4$_APR, χ^2 = 1051 for XCH$_4$_GB, and χ^2 = 451 for XCH$_4$_PST. The estimated uncertainty of the average total emissions for 2010–2011 in the southern Amazon and the central South America regions was 7.9 and 13.3 Tg CH$_4$ yr^{-1} for APR, 7.7 (-2% for APR) and 13.0 Tg CH$_4$ yr^{-1} (-2%) for GB, and 7.0 (-12%) and 11.0 Tg CH$_4$ yr^{-1} (-16%) for PST, respectively. These χ^2 statistics and uncertainty reductions indicate that the satellite and ground-based observations constrain the total CH$_4$ budget more tightly than the ground-based observations alone, due to their regional and global coverage. The precision improvement of flux estimates provides confidence in our interpretation of observed XCH$_4$ variability relative to previous studies that only used ground-based observations. Therefore, the importance of satellite observations for error reduction in inverse modeling is confirmed, especially over regions with fewer ground-based observations, such as the tropics [34].

However, the value of $\chi^2 = 451$ shows that the XCH$_4$_PST distribution is significantly different to that of the XCH$_4$ retrievals ($P < 0.01$), likely due to a combination of factors. The sampling of satellite observations in the southern Amazon region is restricted in the dry season and the spatial distribution differs between 2010 and 2011. These spatio-temporal sampling biases may disturb annual and interannual balances between the dry and wet seasons in the posterior fluxes [35]. The XCH$_4$ retrievals also have a higher scatter than ground-based observations because of the inherent limitations of retrieval algorithms [36] and the detection performance of satellite instruments [12], leading to errors in posterior fluxes. Errors also occur in the models, such as uncertainties in a priori fluxes and in the atmospheric transport model. For instance, the a priori total annual fluxes across the southern Amazon and central South America regions for 2010 were higher than those of CarbonTracker-CH$_4$ (14.1 and 36.3 Tg CH$_4$ yr^{-1}, respectively), although posterior fluxes in CarbonTracker-CH$_4$ were closer to our results (19.9 and 45.8 Tg CH$_4$ yr^{-1}). We assigned a relatively small magnitude to the prior flux uncertainty of biomass burning emissions in order to handle prominent fire events in the 2010 dry season. This means that the posterior flux of biomass burning largely relied on the given prior flux. The choice of prior flux uncertainties is critical for posterior fluxes e.g., [37], and previous studies have investigated methods to characterize the uncertainty e.g., [38–40]. However, statistics related to the uncertainty are not fully understood and remain a major challenge in inversion schemes.

To help interpret differences in XCH$_4$ variability between 2010 and 2011 and dependence of posterior fluxes on prior ones, we ran the inverse model with identical prior fluxes and uncertainties (Table B in S1 File). Instead of prior fluxes with interannual variations, average seasonal cycle of individual emission sources for the period of 2000–2004 were used as identical prior fluxes for both 2010 and 2011. Uncertainties in the identical prior fluxes were set to 20% of the values for the anthropogenic sources and 50% for the natural and biomass burning sources based on GOSAT Level 4 CH$_4$ data product scheme. The results show enhancement of total emissions of 1.4 and 2.6 Tg CH$_4$ yr^{-1} in the southern Amazon and central South America regions in 2010 compared with 2011. The enhancement is mainly related to changes in natural emission sources in posterior fluxes due to the largest uncertainty of prior fluxes in three source groups, and there is no clear difference in biomass burning emissions between 2010 and 2011. Although the inverse model with identical prior fluxes perform less well in this test as shown in small uncertainty reductions, the test reveals the limitation of our ability to quantify biomass burning emissions during Amazonian drought in 2010. As these issues associated with errors in posterior fluxes are difficult to take into account and are key limitations in this study, it should be emphasized that the posterior fluxes can vary with the distribution of satellite sampling, the retrieval algorithms, and the models that were used.

To estimate biomass burning emissions with a different way, we analyzed carbon monoxide (CO) concentrations retrieved from the Measurements Of Pollution In The Troposphere (MOPITT) satellite observations [41] (Fig 2c), as CO serves as a proxy for CH$_4$ emitted during smoldering [42]. Monthly CO levels increased markedly in the southern Amazon region in 2010, peaking at 290–312 ppb (median monthly values) in August and September. Additionally, seasonal variations in the two regions correspond to the ΔXCH$_4$ variations for the two years. These data support the correlation between high-intensity fires and enhanced CH$_4$ emissions by biomass burning in the southern Amazon region during the 2010 drought. Smoke from fires in the region was also detectable by visual inspection of coarse-pixel GOSAT cloud imagery data (Fig D in S1 File).

Globally, wetland CH$_4$ emissions emerge as the primary driver of variability in atmospheric CH$_4$ [43]. In wetlands, the water table depth is a key determinant of emission rates, along with temperature and substrate availability [44]. Increased levels of solar radiation during droughts

may partly increase CH_4 emissions from wetlands, by increasing the amount of substrate available for methanogenesis due to Amazonian forests green-up [45] and increasing temperature in the soil and water. However, during the 2010 drought, low water levels caused by unusually low precipitation resulted in a smaller flooded area [46], thus promoting aerobic soil conditions and reducing CH_4 production. In our estimate, the reduced CH_4 emissions from wetlands caused by the drought occurred beyond the dry season in the southern Amazon region (10.2 ± 4.2 and 11.1 ± 3.9 Tg CH_4 for 2010 and 2011 respectively). Consequently, wetland dynamics is unlikely to explain the enhanced CH_4 emissions in 2010. Drier soil conditions may stimulate termite activity by presenting greater volumes of decaying root biomass, possibly leading to increased CH_4 emissions to the atmosphere. However, a current estimate of global emissions from this source is only ~ 10 Tg CH_4 yr^{-1}, and the emissions in South America account for about 30% of this total [2, 44]. Thus, this contribution alone cannot explain the increased CH_4 emissions of ~ 4.8 Tg CH_4 yr^{-1} in the southern Amazon region in 2010.

Anthropogenic emissions are another important source of atmospheric CH_4. In Brazil, which constitutes the greater part of the southern Amazon region, anthropogenic CH_4 sources are dominated by emissions from ruminants, which in 2005 accounted for 57% (11.5 Tg CH_4 yr^{-1}) of total CH_4 emissions [47]. In Brazil, both total and ruminant emissions decreased slightly from 2005 to 2010, by 6% and 13%, respectively, probably because of the global economic recession. Overall, anthropogenic emissions appear to have a minor influence on the CH_4 budget in the southern Amazon region.

Summary

Although no definite conclusions about CH_4 emissions are possible because of the uncertainty in our estimates, our analyses raise the possibility that severe drought events in 2010 influenced CH_4 emissions in the Amazon. This is apparent as enhanced biomass burning related to land clearing and pasture maintenance [48]. The CH_4 emitted from biomass burning accumulates as greenhouse gases in the atmosphere, which may further enhance the severity and frequency of drought (although drought can also cause a decline in greenhouse gas emissions from tropical soils, via changes in soil redox potential and nutrient availability [49]). The satellite observations provide a solution for mapping XCH_4 distributions over the Amazon region, allowing improvements to our knowledge of the carbon budget. Improvements in data acquirement over cloud-covered areas could lead to further constraints of the CH_4 budget in the region. The overall effects of Amazonian drought on greenhouse gas budgets are not yet fully understood. Further research, such as multi-site investigations of fire regimes and precise ground-based observations of atmospheric CH_4 emissions, are key to improving our understanding the contribution of Amazonian drought to greenhouse gas emissions.

Supporting Information

S1 File. The supplementary materials for this study.
(PDF)

Acknowledgments

obtained from the GOSAT User Interface Gateway at http://www.gosat.nies.go.jp/en/. Maptool uses the Generic Mapping Tools, version 5.2.1 (http://gmt.soest.hawaii.edu/).

Author Contributions

Conceptualization: MS.

Formal analysis: MS HSK.

Funding acquisition: SM TY.

Investigation: MS.

Methodology: MS HSK AI SM.

Project administration: SM TY.

Resources: SM.

Supervision: SM TY.

Validation: HSK.

Visualization: MS.

Writing – original draft: MS.

Writing – review & editing: MS.

References

1. Malhi Y, Wood D, Baker TR, Wright J, Phillips OL, Cochrane T, et al. The regional variation of aboveground live biomass in old-growth Amazonian forests. Global Change Biol. 2006; 12:1107–1138. doi: 10.1111/j.1365-2486.2006.01120.x

2. Kirschke S, Bousquet P, Ciais P, Saunois M, Canadell JG, Dlugokencky EJ, et al. Three decades of global methane sources and sinks. Nature Geosci. 2013; 6:813–823. doi: 10.1038/ngeo1955

3. Marengo JA, Tomasella J, Alves LM, Soares WR, Rodriguez DA. The drought of 2010 in the context of historical droughts in the Amazon region. Geophys Res Lett. 2011; 38. doi: 10.1029/2011GL047436

4. Phillips OL, Aragão LEOC, Lewis SL, Fisher JB, Lloyd J, López-González G, et al. Drought sensitivity of the Amazon rainforest. Science. 2009; 323:1344–1347. doi: 10.1126/science.1164033 PMID: 19265020

5. Gatti LV, Gloor M, Miller JB, Doughty CE, Malhi Y, Domingues LG, et al. Drought sensitivity of Amazonian carbon balance revealed by atmospheric measurements. Nature. 2014; 506:76–80. doi: 10.1038/nature12957 PMID: 24499918

6. Cox PM, Harris PP, Huntingford C, Betts RA, Collins M, Jones CD, et al. Increasing risk of Amazonian drought due to decreasing aerosol pollution. Nature. 2008; 453:212–215. doi: 10.1038/nature06960 PMID: 18464740

7. Melack JM, Hess LL, Gastil M, Forsberg BR, Hamilton SK, Lima IBT, et al. Regionalization of methane emissions in the Amazon Basin with microwave remote sensing. Global Change Biol. 2004; 10:530–544. doi: 10.1111/j.1365-2486.2004.00763.x

8. Yoshida Y, Kikuchi N, Morino I, Uchino O, Oshchepkov S, Bril A, et al. Improvement of the retrieval algorithm for GOSAT SWIR XCO_2 and XCH_4 and their validation using TCCON data. Atmos Meas Tech. 2013; 6:1533–1547. doi: 10.5194/amt-6-1533-2013

9. Tsakiris G, Pangalou D, Vangelis H. Regional drought assessment based on the Reconnaissance Drought Index (RDI). Water Resour Manage. 2007; 21:821–833. doi: 10.1007/s11269-006-9105-4

10. Harris I, Jones PD, Osborn TJ, Lister DH. Updated high-resolution grids of monthly climatic observations–the CRU TS3. 10 Dataset. Int J Climatol. 2014; 34:623–642. doi: 10.1002/joc.3711

11. Yokota T, Yoshida Y, Eguchi N, Ota Y, Tanaka T, Watanabe H, et al. Global concentrations of CO_2 and CH_4 retrieved from GOSAT: first preliminary results. SOLA. 2009; 5:160–163. doi: 10.2151/sola.2009-041

12. Kuze A, Suto H, Nakajima M, Hamazaki T. Thermal and near infrared sensor for carbon observation Fourier-transform spectrometer on the Greenhouse Gases Observing Satellite for greenhouse gases monitoring. Appl Opt. 2009; 48:6716–6733. doi: 10.1364/AO.48.006716

13. Maksyutov S, Takagi H, Valsala VK, Saito M, Oda T, Saeki T, et al. Regional CO_2 flux estimates for 2009–2010 based on GOSAT and ground-based CO_2 observations. Atmos Chem Phys. 2013; 13:9351–9373. doi: 10.5194/acp-13-9351-2013

14. Saeki T, Maksyutov S, Sasakawa M, Machida T, Arshinov M, Tans P, et al. Carbon flux estimation for Siberia by inverse modeling constrained by aircraft and tower CO_2 measurements. J Geophys Res. 2013; 118:1100–1122. doi: 10.1002/jgrd.50127

15. Tsutsumi Y, Mori K, Hirahara T, Ikegami M, Conway TJ. Technical report of global analysis method for major greenhouse gases by the World Data Center for Greenhouse Gases. World Meteorological Organization; 2009.

16. Sasakawa M, Machida T, Tsuda N, Arshinov M, Davydov D, Fofonov A, et al. Aircraft and tower measurements of CO_2 concentration in the planetary boundary layer and the lower free troposphere over southern taiga in West Siberia: Long-term records from 2002 to 2011. J Geophys Res. 2013; 118:9489–9498. doi: 10.1002/jgrd.50755

17. Bergamaschi P, Frankenberg C, Meirink JF, Krol M, Villani MG, Houweling S, et al. Inverse modeling of global and regional CH_4 emissions using SCIAMACHY satellite retrievals. J Geophys Res. 2009; 114. doi: 10.1029/2009JD012287

18. Kim HS, Maksyutov S, Glagolev MV, Machida T, Patra PK, Sudo K, et al. Evaluation of methane emissions from West Siberian wetlands based on inverse modeling. Environ Res Lett. 2011; 6:035201. doi: 10.1088/1748-9326/6/3/035201

19. GLOBALVIEW-CH_4. Cooperative Atmospheric Data Integration Project–Carbon Dioxide; 2009.

20. Patra PK, Houweling S, Krol M, Bousquet P, Belikov D, Bergmann D, et al. TransCom model simulations of CH_4 and related species: linking transport, surface flux and chemical loss with CH_4 variability in the troposphere and lower stratosphere. Atmos Chem Phys. 2011; 11:12813–12837. doi: 10.5194/acp-11-12813-2011

21. Bruhwiler LMP, Michalak AM, Peters W, Baker DF, Tans P. An improved Kalman Smoother for atmospheric inversions. Atmos Chem Phys. 2005; 5:2691–2702. doi: 10.5194/acp-5-2691-2005

22. Onogi K, Tsutsui J, Koide H, Sakamoto M, Kobayashi S, Hatsushika H, et al. The JRA-25 Reanalysis. J Meteorol Soc Jap. 2007; 85:369–432. doi: 10.2151/jmsj.85.369

23. European Commission Joint Research Centre, Netherlands Environmental Assessment Agency. Emission Database for Global Atmospheric Research (EDGAR), Release Version 4.2.; 2010.

24. Ito A, Inatomi M. Use of a process-based model for assessing the methane budgets of global terrestrial ecosystems and evaluation of uncertainty. Biogeosciences. 2012; 9:759–773. doi: 10.5194/bg-9-759-2012

25. Fung I, John J, Lerner J, Matthews E, Prather M, Steele LP, et al. Three-dimensional model synthesis of the global methane cycle. J Geophys Res. 1991; 96:13033–13065. doi: 10.1029/91JD01247

26. Van der Werf GR, Randerson JT, Giglio L, Collatz GJ, Mu M, Kasibhatla PS, et al. Global fire emissions and the contribution of deforestation, savanna, forest, agricultural, and peat fires (1997–2009). Atmos Chem Phys. 2010; 10(23):11707–11735. doi: 10.5194/acp-10-11707-2010

27. Frankenberg C, Meirink JF, van Weele M, Platt U, Wagner T. Assessing Methane Emissions from Global Space-Borne Observations. Science. 2005; 308(5724):1010–1014. doi: 10.1126/science.1106644 PMID: 15774724

28. Miller JB, Gatti LV, d'Amelio MTS, Crotwell AM, Dlugokencky EJ, Bakwin P, et al. Airborne measurements indicate large methane emissions from the eastern Amazon basin. Geophys Res Lett. 2007; 34. doi: 10.1029/2006GL029213

29. Marengo JA, Soares WR, Saulo C, Nicolini M. Climatology of the low-level jet east of the Andes as derived from the NCEP-NCAR reanalyses: Characteristics and temporal variability. J climate. 2004; 17:2261–2280. doi: 10.1175/1520-0442(2004)017%3C2261:COTLJE%3E2.0.CO;2

30. Potter C, Brooks-Genovese V, Klooster S, Torregrosa A. Biomass burning emissions of reactive gases estimated from satellite data analysis and ecosystem modeling for the Brazilian Amazon region. J Geophys Res. 2002; 107(D20):LBA–23. doi: 10.1029/2000JD000250

31. Guild LS, Kauffman JB, Cohen WB, Hlavka CA, Ward DE. Modeling biomass burning emissions for Amazon forest and pastures in Rondônia, Brazil. Eco Appl. 2004; 14:232–246. doi: 10.1890/01-6009

32. Bruhwiler L, Dlugokencky E, Masarie K, Ishizawa M, Andrews A, Miller J, et al. CarbonTracker-CH_4: an assimilation system for estimating emissions of atmospheric methane. Atmos Chem Phys. 2014; 14 (16):8269–8293. doi: 10.5194/acp-14-8269-2014

33. Wilson C, Gloor M, Gatti LV, Miller JB, Monks SA, McNorton J, et al. Contribution of regional sources to atmospheric methane over the Amazon Basin in 2010 and 2011. Global Biogeochem Cycles. 2016;.

34. Fraser A, Palmer PI, Feng L, Boesch H, Cogan A, Parker R, et al. Estimating regional methane surface fluxes: the relative importance of surface and GOSAT mole fraction measurements. Atmos Chem Phys. 2013; 13:5697–5713. doi: 10.5194/acp-13-5697-2013

35. Liu J, Bowman KW, Lee M, Henze DK, Bousserez N, Brix H, et al. Carbon monitoring system flux estimation and attribution: impact of ACOS-GOSAT X_{CO2} sampling on the inference of terrestrial biospheric sources and sinks. Tellus B. 2014; 66:22486. doi: 10.3402/tellusb.v66.22486

36. Dils B, Buchwitz M, Reuter M, Schneising O, Boesch H, Parker R, et al. The Greenhouse Gas Climate Change Initiative (GHG-CCI): comparative validation of GHG-CCI SCIAMACHY/ENVISAT and TANSO-FTS/GOSAT CO_2 and CH_4 retrieval algorithm products with measurements from the TCCON. Atmos Meas Tech. 2014; 7(6):1723–1744. doi: 10.5194/amt-7-1723-2014

37. Law RM, Rayner PJ, Steele LP, Enting IG. Using high temporal frequency data for CO_2 inversions. Global biogeochem cycles. 2002; 16:1053. doi: 10.1029/2001GB001593

38. Chapnik B, Desroziers G, Rabier F, Talagrand O. Properties and first application of an error-statistics tuning method in variational assimilation. Q J R Meteorol Soc. 2004; 130(601):2253–2275. doi: 10.1256/qj.03.26

39. Berchet A, Pison I, Chevallier F, Bousquet P, Conil S, Geever M, et al. Towards better error statistics for atmospheric inversions of methane surface fluxes. Atmos Chem Phys. 2013; 13:7115–7132. doi: 10.5194/acp-13-7115-2013

40. Ganesan AL, Rigby M, Zammit-Mangion A, Manning AJ, Prinn RG, Fraser PJ, et al. Characterization of uncertainties in atmospheric trace gas inversions using hierarchical Bayesian methods. Atmos Chem Phys. 2014; 14:3855–3864. doi: 10.5194/acp-14-3855-2014

41. Deeter MN, Emmons LK, Francis GL, Edwards DP, Gille JC, Warner JX, et al. Operational carbon monoxide retrieval algorithm and selected results for the MOPITT instrument. J Geophys Res. 2003; 108 (D14). doi: 10.1029/2002JD003186

42. Crutzen PJ, Andreae MO. Biomass Burning in the Tropics: Impact on Atmospheric Chemistry and Biogeochemical Cycles. Science. 1990; 250(4988):1669–1678. doi: 10.1126/science.250.4988.1669 PMID: 17734705

43. Bousquet P, Ciais P, Miller JB, Dlugokencky EJ, Hauglustaine DA, Prigent C, et al. Contribution of anthropogenic and natural sources to atmospheric methane variability. Nature. 2006; 443:439–443. doi: 10.1038/nature05132 PMID: 17006511

44. Christensen TR. Wetlands. In: Reay D, Smith P, van Amstel A, editors. Methane and Climate Change. Earthscan; 2010. p. 27–41.

45. Saleska SR, Didan K, Huete AR, Da Rocha HR. Amazon forests green-up during 2005 drought. Science. 2007; 318:612–612. doi: 10.1126/science.1146663 PMID: 17885095

46. Arnesen AS, Silva TSF, Hess LL, Novo EM, Rudorff CM, Chapman BD, et al. Monitoring flood extent in the lower Amazon River floodplain using ALOS/PALSAR ScanSAR images. Remote Sens Environ. 2013; 130:51–61. doi: 10.1016/j.rse.2012.10.035

47. EPA. Global Anthropogenic Non-CO_2 Greenhouse Gas Emissions: 1990–2030; 2012.

48. Fearnside PM. Fire in the tropical rain forest of the Amazon basin. In: Goldammer JG, editor. Fire in the tropical biota. Springer; 1990. p. 106–116. doi: 10.1007/978-3-642-75395-4_7

49. Wood TE, Silver WL. Strong spatial variability in trace gasdynamics following experimental drought in a humid tropical forest. Global Biogeochem Cycles. 2012; 26:GB3005. doi: 10.1029/2010GB004014